Partitioned algorithms for the solution of fluid-structure interaction problems for real applications in haemodynamics

Fabio Nobile[1], Matteo Pozzoli[2], and Christian Vergara[3]

1 MATHICSE, EPFL, Station 8, 1015 Lausanne, Switzerland
MOX, Dipartimento di Matematica, Politecnico di Milano
Piazza Leonardo da Vinci 32, 20133, Milan, Italy,
`fabio.nobile@polimi.it`
3 Dipartimento di Ingegneria dell'Informazione e Metodi Matematici, Univerità di Bergamo
Viale Marconi 5, 24044, Dalmine (BG), Italy,
`christian.vergara@unibg.it`

2 MOX, Dipartimento di Matematica, Politecnico di Milano
Piazza Leonardo da Vinci 32, 20133, Milan, Italy,
`matteo.pozzoli@mail.polimi.it`

Abstract

In this work we deal with the numerical solution of the fluid-structure interaction problem arising in the haemodynamic environment. In particular, we consider BDF time discretization schemes, and we study different methods for the treatment of the fluid-structure interface position, focusing on partitioned algorithms. We consider explicit and implicit algorithms, and new hybrid methods. We study numerically the performances and the accuracy of these schemes, highlighting the best solutions for haemodynamic applications.

Keywords: Fluid-structure interaction, blood flow, BDF schemes, partitioned schemes.

Introduction

Building efficient strategies for the solution of the fluid-structure interaction (FSI) problem is a major issue in *computational haemodynamics*. In particular here we are interested in the FSI problem arising by the interaction between the blood flow and the vessel wall deformation (see, e.g., [2, 5, 11, 13, 24, 26]). The main difficulties related to the numerical solution of the FSI problem are: *(i)* the treatment of the *interface position*, since the fluid domain is an unknown of the problem (*geometrical non-linearity*); *(ii)* the treatment of the *interface continuity conditions*, which enforce continuity of velocities and normal stresses between fluid and structure; *(iii)* the fact that the subproblems could be non-linear (*physical non-linearities*). These features make the FSI problem a strongly non-linear coupled problem, as there is a substantial amount of energy exchanged between fluid and structure in each cardiac beat. This non-linear behaviour is essentially related to points *(i)* and *(ii)* above. Therefore, in this work we focus mainly on these two points. Regarding the third point, we consider just the fluid non-linearity due to the convective term in the Navier-Stokes equations, and we consider a linear structure.

Concerning the first point, we can mainly detect two strategies: an *implicit treatment* of the interface position or an *explicit treatment*, thanks to extrapolations of the solu-

tion at previous time steps.

After a suitable linearization of the physical non-linearities, whichever of the two strategies is adopted for the treatment of the interface position (implicit or explicit), one has to deal with a *linearized* FSI problem (in the sense that we have eliminated the geometrical and physical non-linearities). However, this problem is still coupled through the interface continuity conditions. For the solution of this linearized FSI problem we consider partitioned schemes, where one solves the fluid and structure subproblems in an iterative framework, until fulfillment of the interface continuity conditions (see, e.g., [2, 6, 8, 14, 25]).

The goal of this work is to compare the accuracy and performances of different treatments of the FS interface position, when partitioned procedures are considered for the enforcement of the continuity conditions. To this aim, we consider an application of such schemes to a patient-specific case.

The continuous FSI problem

Let us consider an open domain $\Omega_f^t \subset \mathbb{R}^3$ like the one represented in Figure 1 (on the left). This represents the lumen of a vessel and it is function of time t. Inflow and outflow sections are denoted by $\Sigma_{f,i}^t$ (three in Figure 1). Blood velocity is denoted by $\boldsymbol{u}_f(\boldsymbol{x}, t)$, the pressure by $p_f(\boldsymbol{x}, t)$. The incompressible Navier-Stokes equations for a Newto-
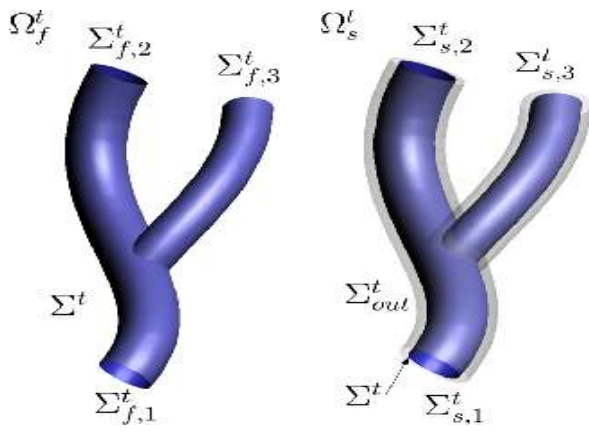
Figure 1 Representation of the domain of the FSI problem: fluid domain on the left, structure domain on the right.

nian fluid are assumed to hold in Ω_f^t. Let $\boldsymbol{T}_f$ be the related Cauchy stress tensor defined by

$$\boldsymbol{T}_f(\boldsymbol{u}_f, p_f) := -p_f \boldsymbol{I} + \mu(\nabla \boldsymbol{u}_f + (\nabla \boldsymbol{u}_f)^T).$$

Since we work in a moving domain, the fluid problem is stated in an *Arbitrary Lagrangian-Eulerian* (ALE) framework (see e.g. [9, 18]). The ALE map $\mathcal{A}$ is defined by an appropriate lifting of the structure displacement at the FS interface Σ^t, and defines the displacement of the points of the fluid domain $\boldsymbol{\eta}_m$ and their velocity $\boldsymbol{u}_m$. For any function v living in the current fluid configuration, we denote by $\widetilde{v} := v \circ \mathcal{A}$ its counterpart in the reference configuration. A classical choice in haemodynamic applications to define the ALE map is to consider a harmonic extension operator in the reference domain (see, e.g., [21]).

The vessel wall is denoted by Ω_s^t, which is an open subset of $\mathbb{R}^3$ (see Figure 1, right). The intersection of Ω_s^t and Ω_f^t is empty, and $\Sigma^t := \bar{\Omega}_s^t \cup \bar{\Omega}_f^t$ is the FS interface. On Σ^t we define a normal unit vector $\boldsymbol{n}$ poiting outward of the solid domain and inward to the fluid domain. The inflow/outflow sections (three in Figure 1) are denoted by $\Sigma_{s,i}^t$. With Σ_{out}^t we denote the external surface of the structure domain. We denote by $\boldsymbol{\eta}_s(\boldsymbol{x}, t)$ the wall displacement. We assume that the solid is a linear elastic material, characterized by the following Piola-Kirchhoff stress tensor

$$\widetilde{\boldsymbol{T}}_s = \frac{E}{2(1+\nu)} \boldsymbol{\epsilon}(\widetilde{\boldsymbol{\eta}}_s) + \frac{E\nu}{(1+\nu)(1-2\nu)} \operatorname{tr}(\boldsymbol{\epsilon}(\widetilde{\boldsymbol{\eta}}_s)) \boldsymbol{I},$$

where $\boldsymbol{\epsilon}(\boldsymbol{\eta}) := \frac{(\nabla\boldsymbol{\eta} + (\nabla\boldsymbol{\eta})^T)}{2}$, E is the Young modulus, and ν is the Poisson ratio. To describe the structure kinematics we adopt a purely Lagrangian approach, where $\mathcal{L}$ is the Lagrangian map. For any function g defined in the current solid configuration Ω_s^t, we denote by $\widetilde{g} := g \circ \mathcal{L}$ its counterpart in the reference domain.

The strong formulation of the FSI problem, including the computation of the ALE map, reads therefore as follows

1. *Fluid-Structure problem.* Given the (unknown) fluid domain velocity $\boldsymbol{u}_m$ and fluid domain Ω_f^t, find, at

each time $t \in (0, T]$, fluid velocity $\boldsymbol{u}_f$, pressure p_f and structure displacement $\boldsymbol{\eta}_s$ such that

$$\begin{cases} \rho_f \dfrac{D^A \boldsymbol{u}_f}{Dt} + \rho_f((\boldsymbol{u}_f - \boldsymbol{u}_m) \cdot \nabla)\boldsymbol{u}_f & \\ \quad -\nabla \cdot \boldsymbol{T}_f(\boldsymbol{u}_f, p_f) = \boldsymbol{f}_f & \text{in } \Omega_f^t, \\ \nabla \cdot \boldsymbol{u}_f = 0 & \text{in } \Omega_f^t, \\ \rho_s \dfrac{\partial^2 \widetilde{\boldsymbol{\eta}}_s}{\partial t^2} - \nabla \cdot \widetilde{\boldsymbol{T}}_s(\widetilde{\boldsymbol{\eta}}_s) = \widetilde{\boldsymbol{f}}_s & \text{in } \Omega_s^0, \\ \boldsymbol{u}_f = \dfrac{\partial \boldsymbol{\eta}_s}{\partial t} & \text{on } \Sigma^t, \\ \boldsymbol{T}_s(\boldsymbol{\eta}_s)\,\boldsymbol{n} - \boldsymbol{T}_f(\boldsymbol{u}_f, p_f)\,\boldsymbol{n} = \boldsymbol{0} & \text{on } \Sigma^t, \\ \alpha_e \widetilde{\boldsymbol{\eta}}_s + \widetilde{\boldsymbol{T}}_s(\widetilde{\boldsymbol{\eta}}_s)\,\widetilde{\boldsymbol{n}} = P_{ext}\widetilde{\boldsymbol{n}}, & \text{on } \Sigma_{out}^0, \end{cases} \tag{1}$$

where D^A/Dt is the ALE time derivative, ρ_f and ρ_s are the fluid and structure densities, μ is the constant blood viscosity, $\boldsymbol{f}_f$ and $\boldsymbol{f}_s$ the forcing terms;

2. *Geometry problem.* Given the (unknown) interface structure displacement $\widetilde{\boldsymbol{\eta}}_s|_{\Sigma^0}$, find the displacement of the points of the fluid domain $\boldsymbol{\eta}_m$ such that

$$\begin{cases} -\triangle\widetilde{\boldsymbol{\eta}}_m = \boldsymbol{0} & \text{on } \Omega_f^0, \\ \widetilde{\boldsymbol{\eta}}_m = \widetilde{\boldsymbol{\eta}}_s & \text{on } \Sigma^0, \end{cases} \tag{2}$$

and then find accordingly the fluid domain velocity $\widetilde{\boldsymbol{u}}_m := \frac{\partial \widetilde{\boldsymbol{\eta}}_m}{\partial t}$, and the new points $\boldsymbol{x}_f^t$ of the fluid domain by moving the points $\boldsymbol{x}_f^0$ of the reference domain Ω_f^0:

$$\boldsymbol{x}_f^t = \boldsymbol{x}_f^0 + \widetilde{\boldsymbol{\eta}}_m.$$

The two matching conditions enforced at the interface are the *continuity of velocities* $(1)_4$ and the *continuity of normal stresses* $(1)_5$. The fluid and structure are also coupled by the geometry problem, leading to a highly nonlinear system of partial differential equations. Equations (1) and (2) have to be endowed with suitable boundary conditions on $\Omega_f^t \setminus \Sigma^t$ and $\Omega_s^0 \setminus (\Sigma^0 \cup \Sigma_{out}^0)$, and with suitable initial conditions. We prescribe the Robin boundary condition $(1)_6$ on Σ_{out}^0, with the aim of modeling the presence of a surrounding tissue around the vessel. This choice corresponds to consider an elastic behaviour of this tissue, where α_e is the corresponding elastic coefficient (see [19, 20]).

Time discretization of the FSI problem

Let Δt be the time discretization parameter and $t^n := n\,\Delta t$, $n = 0, 1, \ldots$. For a generic function z, with z^n we denote the approximation of $z(t^n)$. In this work we consider *Backward Differentiation Formulae* (BDF) schemes (see [16, 17]). We propose in what follows the discrete-in-time formulation of the time discrete problem (1)-(2).

1. *Fluid-Structure problem.* Given the (unknown) fluid domain velocity $\boldsymbol{u}_m^{n+1}$ and the fluid domain Ω_f^{n+1}, the parameters $\beta_{f,i}(i = 0, \ldots, p)$, χ_f, $\beta_{s,i}(i = 0, \ldots, p)$, σ_s, ζ_s, $\xi_{s,i}(i = 0, \ldots, p+1)$, χ_s, κ_s,

the solution at previous time steps, and functions $\boldsymbol{f}_f^{n+1}$, $\boldsymbol{f}_s^{n+1}$ and P_{ext}, find fluid velocity $\boldsymbol{u}_f^{n+1}$, pressure p_f^{n+1} and structure displacement $\boldsymbol{\eta}_s^{n+1}$ such that [22]

$$\begin{cases} \rho_f \dfrac{\beta_{f,0}}{\Delta t}\boldsymbol{u}_f^{n+1} \\ \quad + \rho_f((\boldsymbol{u}_f^{n+1} - \boldsymbol{u}_m^{n+1})\cdot\nabla)\boldsymbol{u}_f^{n+1} \\ \quad -\nabla\cdot\boldsymbol{T}_f^{n+1} = \boldsymbol{f}_f^{n+1} + \rho_f\boldsymbol{f}_{f,W}^{n+1} & \text{in } \Omega_f^{n+1}, \\ \nabla\cdot\boldsymbol{u}_f^{n+1} = 0 & \text{in } \Omega_f^{n+1}, \\ \rho_s \dfrac{\xi_{s,0}}{\Delta t^2}\widetilde{\boldsymbol{\eta}}_s^{n+1} - \nabla\cdot\widetilde{\boldsymbol{T}}_s^{n+1}(\widetilde{\boldsymbol{\eta}}_s^{n+1}) \\ \quad = \widetilde{\boldsymbol{f}}_s^{n+1} + \rho_s\widetilde{\boldsymbol{f}}_{s,W}^{n+1} & \text{in } \Omega_s^0, \\ \boldsymbol{u}_f^{n+1} = \boldsymbol{u}_s^{n+1} & \text{on } \Sigma^{n+1}, \\ \boldsymbol{T}_s^{n+1}(\boldsymbol{\eta}_s^{n+1})\,\boldsymbol{n} \\ \quad -\boldsymbol{T}_f^{n+1}(\boldsymbol{u}_f^{n+1},p_f^{n+1})\,\boldsymbol{n} = \boldsymbol{0} & \text{on } \Sigma^{n+1}, \\ \alpha_e\widetilde{\boldsymbol{\eta}}_s^{n+1} + \widetilde{\boldsymbol{T}}_s^{n+1}(\widetilde{\boldsymbol{\eta}}_s^{n+1})\,\widetilde{\boldsymbol{n}} = P_{ext}\widetilde{\boldsymbol{n}} & \text{on } \Sigma_{out}^0, \end{cases}$$
$$(3)$$

where

$$\boldsymbol{f}_{s,U}^{n+1} := \sum_{i=1}^{p} \frac{\beta_{s,i}}{\Delta t}\boldsymbol{\eta}_s^{n+1-i},$$

$$\boldsymbol{f}_{s,W}^{n+1} := \sum_{i=1}^{p+1} \frac{\xi_{s,i}}{\Delta t^2}\boldsymbol{\eta}_s^{n+1-i},$$

$$\boldsymbol{f}_{f,W}^{n+1} := \sum_{i=1}^{p} \frac{\beta_{f,i}}{\Delta t}\boldsymbol{u}_f^{n+1-i},$$

are the forcing terms coming from the time discretization. In problem (3) we have also introduced the structure velocity $\boldsymbol{u}_s^n := \frac{\beta_{s,0}}{\Delta t}\boldsymbol{\eta}_s^n - \boldsymbol{f}_{s,U}^n$, the structure acceleration $\boldsymbol{w}_s^n := \frac{\xi_{s,0}}{\Delta t^2}\boldsymbol{\eta}_s^n - \boldsymbol{f}_{s,W}^n$, and the fluid acceleration $\boldsymbol{w}_f^n := \frac{\beta_{f,0}}{\Delta t}\boldsymbol{u}_f^n - \boldsymbol{f}_{f,W}^n$.

2. *Geometry problem.* Given the (unknown) interface structure displacement $\widetilde{\boldsymbol{\eta}}_s^{n+1}|_{\Sigma^0}$, solve a harmonic extension problem

$$\begin{cases} -\triangle\widetilde{\boldsymbol{\eta}}_m^{n+1} = \boldsymbol{0} & \text{in } \Omega_f^0, \\ \widetilde{\boldsymbol{\eta}}_m^{n+1} = \widetilde{\boldsymbol{\eta}}_s^{n+1} & \text{on } \Sigma^0, \end{cases} \qquad (4)$$

and then find accordingly the discrete fluid domain velocity

$$\widetilde{\boldsymbol{u}}_m^{n+1} := \frac{\beta_{s,0}}{\Delta t}\widetilde{\boldsymbol{\eta}}_m^{n+1} - \widetilde{\boldsymbol{f}}_{m,U}^{n+1}, \qquad (5)$$

and the points $\boldsymbol{x}_f^{n+1}$ of the new fluid domain by $\boldsymbol{x}_f^{n+1} = \boldsymbol{x}_f^0 + \widetilde{\boldsymbol{\eta}}_m^{n+1}$. Here $\widetilde{\boldsymbol{f}}_{m,U}^{n+1}$, $\widetilde{\boldsymbol{w}}_m^{n+1}$ and $\widetilde{\boldsymbol{f}}_{m,W}^{n+1}$ (the last two quantities are needed for the computation of $\widetilde{\boldsymbol{f}}_{m,U}^{n+1}$) are obtained using the same formulae as for $\boldsymbol{f}_{s,U}$, $\boldsymbol{w}_s$ and $\boldsymbol{f}_{s,W}$. Observe that $(4)_2$ guarantees that the displacement of the fluid interface coincides with that of the structure (geometrical conformity), whereas (5) guarantees that also the mesh and structure velocities coincide at the FS interface.

A Lagrange multipliers-based formulation

In order to introduce suitable algorithms for the numerical solution of (3) and (4), we consider here an equivalent formulation based on the introduction of three Lagrange multipliers living at the FS interface, representing the fluid and structure normal stresses $\boldsymbol{\lambda}_f$ and $\boldsymbol{\lambda}_s$, and the normal derivative of the fluid mesh displacement $\boldsymbol{\lambda}_m$ (see [22]). These new unknowns are introduced just to simplify the expression of the three interface continuity conditions $(3)_{4-5}$ and $(4)_2$, and the derivation of the partitioned algorithms. However, we have not introduced them in our practical implementation of the algorithms to avoid extra costs.

We start by introducing some new notations. For the sake of notation we remove the temporal index $^{n+1}$. Given a space W, we denote with W^* its dual, with Σ_f^D and Σ_m^D we denote the parts of the boundary $\partial\Omega_f \setminus \Sigma$ where Dirichlet boundary conditions are prescribed for the fluid subproblem and for the harmonic extension problem, respectively, and with $\Sigma_s^{D,0}$ the part of $\partial\Omega_s^0 \setminus \Sigma^0$ where Dirichlet conditions are prescribed for the structure subproblem. Then, we define the following spaces

$$V_f := \{v \in H^1(\Omega_f) :\ v|_{\Sigma_f^D} = 0\}, \qquad Q := L^2(\Omega_f),$$

$$V_s := \{v \in H^1(\Omega_s^0) :\ v|_{\Sigma_s^{D,0}} = 0\},$$

$$V_m := \{v \in H^1(\Omega_f^0) :\ v|_{\Sigma_m^{D,0}} = 0\}.$$

Let $\mathcal{F} : [V_f]^3 \times Q \times [V_m]^3 \to ([V_f]^3 \times Q)^*$ be the fluid operator and $\mathcal{G}_f$ be the operator related to the right hand side of the fluid equations. Analogously, for the structure subproblem we introduce the operator $\mathcal{S} : [V_s]^3 \to ([V_s]^3)^*$ and $\mathcal{G}_s$. Finally, for the harmonic extension, we introduce the operator $\mathcal{H} : [V_m]^3 \to ([V_m]^3)^*$. For the definitions of the above operators, we refer the reader to [22]. We also define the following trace operators

$$\begin{aligned} \widetilde{\gamma}_f &: [V_f]^3 \to [H^{1/2}(\Sigma^0)]^3, \ \widetilde{\gamma}_f\boldsymbol{v} := \widetilde{\boldsymbol{v}}|_{\Sigma^0}, \\ \widetilde{\gamma}_s &: [V_s]^3 \to [H^{1/2}(\Sigma^0)]^3, \ \widetilde{\gamma}_s\widetilde{\boldsymbol{\mu}} := \widetilde{\boldsymbol{\mu}}|_{\Sigma^0}, \\ \widetilde{\gamma}_m &: [V_m]^3 \to [H^{1/2}(\Sigma^0)]^3, \ \widetilde{\gamma}_m\widetilde{\boldsymbol{z}} := \widetilde{\boldsymbol{z}}|_{\Sigma^0}, \end{aligned} \qquad (6)$$

and the related adjoint operators.

We are now ready to rewrite problem (3)-(4) as follows

$$\begin{cases} \mathcal{H}(\widetilde{\boldsymbol{\eta}}_m) + \widetilde{\gamma}_m^*\widetilde{\boldsymbol{\lambda}}_m = \boldsymbol{0} & \text{in } ([V_m]^3)^*, \\ \widetilde{\gamma}_m\widetilde{\boldsymbol{\eta}}_m = \widetilde{\gamma}_s\widetilde{\boldsymbol{\eta}}_s & \text{on } \Sigma^0, \\ \mathcal{F}(\boldsymbol{u}_f,p_f,\boldsymbol{u}_m) + \widetilde{\gamma}_f^*\widetilde{\boldsymbol{\lambda}}_f = \mathcal{G}_f & \text{in } ([V_f]^3)^*, \\ \alpha_f\,\widetilde{\gamma}_f\boldsymbol{u}_f + \widetilde{\boldsymbol{\lambda}}_f \\ \quad = \alpha_f\widetilde{\gamma}_s\left(\frac{\beta_{s,0}}{\Delta t}\widetilde{\boldsymbol{\eta}}_s - \widetilde{\boldsymbol{f}}_{s,U}\right) - \widetilde{\boldsymbol{\lambda}}_s & \text{on } \Sigma^0, \\ \alpha_s\widetilde{\gamma}_s\frac{\beta_{s,0}}{\Delta t}\widetilde{\boldsymbol{\eta}}_s + \widetilde{\boldsymbol{\lambda}}_s \\ \quad = \alpha_s\widetilde{\gamma}_f\boldsymbol{u}_f - \widetilde{\boldsymbol{\lambda}}_f + \alpha_s\widetilde{\gamma}_s\widetilde{\boldsymbol{f}}_{s,U} & \text{on } \Sigma^0, \\ \mathcal{S}(\widetilde{\boldsymbol{\eta}}_s) + \widetilde{\gamma}_s^*\widetilde{\boldsymbol{\lambda}}_s = \mathcal{G}_s & \text{in } ([V_s]^3)^*, \end{cases}$$
$$(7)$$

where the interface continuity conditions $(7)_{4-5}$ are linear combinations of conditions $(3)_{4-5}$, through the introduction of two functions in $L^\infty(\Sigma^0)$, $\alpha_f \neq \alpha_s$. This will

be useful to derive partitioned procedures based on Robin interface conditions (Robin-Robin (RR) schemes, see [1–3, 15]). This approach has good convergence properties, independent of the added-mass effect (which is very high in haemodynamic contexts, see [6]) when the parameters α_f and α_s are suitably chosen, as shown in [2, 15].

In [22] it has been shown that the Lagrange multiplier $\boldsymbol{\lambda}_f$ and $\boldsymbol{\lambda}_s$ have the physical meaning of the fluid and structure normal stress at the FS interface *in the reference configuration*.

Numerical algorithms

For the solution of the FSI problem (7), we propose to use a general preconditioned Richardson method

$$\widehat{F}(y^k)\,\delta y^{k+1} = -F(y^k), \qquad (8)$$

where y^k denotes the FSI solution $[\widetilde{\boldsymbol{\eta}}_m^k, \widetilde{\boldsymbol{\lambda}}_m^k, \boldsymbol{v}_f^k, \widetilde{\boldsymbol{\lambda}}_f^k, \widetilde{\boldsymbol{\lambda}}_s^k, \widetilde{\boldsymbol{\eta}}_s^k]$ at the generic subiteration k, with $\boldsymbol{v}_f := (\boldsymbol{u}_f, p_f)$, δy^{k+1} is the increment of the FSI solution at the new iteration $k+1$ with respect to y^k, $F(y) = 0$ corresponds to problem (7), and $\widehat{F}$ is a suitable preconditioner.

In this work, we consider quasi-Newton methods. In particular, we consider the following approximation of the exact jacobian [22]

$$\widehat{F} = \begin{bmatrix} \mathcal{H} & \widetilde{\gamma}_m^* & & & & -\widetilde{\gamma}_s \\ \widetilde{\gamma}_m & & & & & \\ \hline & & \widehat{\nabla}_{v_f}\mathcal{F} & \widetilde{\gamma}_f^* & & \\ & & \alpha_f\widetilde{\gamma}_f & I & I & -\alpha_f\frac{\beta_{s,0}}{\Delta t}\widetilde{\gamma}_s \\ \hline & & -\alpha_s\widetilde{\gamma}_f & I & I & \alpha_s\frac{\beta_{s,0}}{\Delta t}\widetilde{\gamma}_s \\ & & & & \widetilde{\gamma}_s^* & \mathcal{S} \end{bmatrix},$$

where $\widehat{\nabla}_{v_f}\mathcal{F}$ is obtained from $\nabla_{v_f}\mathcal{F}$ by skipping the term $(\delta\boldsymbol{u}_f \cdot \nabla)\boldsymbol{u}_f$ [22]. Moreover, we do not consider the shape derivatives $\nabla_{u_m}\mathcal{F}$. This leads to the Oseen approximation of the Navier-Stokes problem obtained by using as convective term previous solutions $\boldsymbol{u}_f$ and $\boldsymbol{u}_m$.

We are ready now to derive from $\widehat{F}$ another preconditioner, leading to suitable algorithms for the numerical solution of (7). Since the structure is linear, we report these algorithms in non-incremental form.

Double-loop algorithm

We consider the following *two block Gauss-Seidel* preconditioner

$$\widehat{J}_{DL} = \begin{bmatrix} \mathcal{H} & \widetilde{\gamma}_m^* & & & & \\ \widetilde{\gamma}_m & & & & & \\ \hline & & \widehat{\nabla}_{v_f}\mathcal{F} & \widetilde{\gamma}_f^* & & \\ & & \alpha_f\widetilde{\gamma}_f & I & I & -\alpha_f\frac{\beta_{s,0}}{\Delta t}\widetilde{\gamma}_s \\ \hline & & -\alpha_s\widetilde{\gamma}_f & I & I & \alpha_s\frac{\beta_{s,0}}{\Delta t}\widetilde{\gamma}_s \\ & & & & \widetilde{\gamma}_s^* & \mathcal{S} \end{bmatrix},$$

which corresponds to the sequential solution of the harmonic extension and of a linearized FSI problem. For the solution of the latter, since we are interested in partitioned algorithms, we use the following preconditioner (see [2])

$$\widehat{P}_{RR} = \begin{bmatrix} \widehat{\nabla}_{v_f}\mathcal{F} & \widetilde{\gamma}_f^* & & \\ \alpha_f\widetilde{\gamma}_f & I & & \\ \hline -\alpha_s\widetilde{\gamma}_f & I & I & \alpha_s\frac{\beta_{s,0}}{\Delta t}\widetilde{\gamma}_s \\ & & \widetilde{\gamma}_s^* & \mathcal{S} \end{bmatrix}.$$

This corresponds to consider two nested loops, an external one for the treatment of the interface position through a fixed-point (quasi-Newton) scheme, and an internal one for the treatment of the interface continuity conditions through the RR scheme. In particular, we have the following algorithm:

Given the solution at iteration k, solve at the current iteration $k+1$ until convergence (we omit the superscript $k+1$)

1. The harmonic extension

$$\begin{cases} -\triangle\widetilde{\boldsymbol{\eta}}_m = \boldsymbol{0} & \text{in } \Omega_f^0, \\ \widetilde{\gamma}_m\,\widetilde{\boldsymbol{\eta}}_m = \widetilde{\gamma}_s\,\widetilde{\boldsymbol{\eta}}_s^k & \text{on } \Sigma^0, \end{cases}$$

obtaining the new fluid domain Ω_f and the fluid domain velocity $\boldsymbol{u}_m$.

2. The linearized FSI problem. In particular, given the solution at subiteration $l-1$, solve at the current subiteration l until convergence

   (a) The fluid subproblem with a Robin condition at the FS interface

$$\begin{cases} \rho_f\dfrac{\beta_{f,0}}{\Delta t}\boldsymbol{u}_{f,l} + \rho_f((\boldsymbol{u}_f^k - \boldsymbol{u}_m)\cdot\nabla)\boldsymbol{u}_{f,l} \\ \qquad -\nabla\cdot\boldsymbol{T}_{f,l} = \boldsymbol{f}_f + \rho_f\boldsymbol{f}_{f,W} & \text{in } \Omega_f, \\ \nabla\cdot\boldsymbol{u}_{f,l} = 0 & \text{in } \Omega_f, \\ \alpha_f\,\gamma_f\,\boldsymbol{u}_{f,l} + \boldsymbol{T}_{f,l} \\ \qquad = \alpha_f\gamma_s\left(\dfrac{\beta_{s,0}}{\Delta t}\boldsymbol{\eta}_{s,l-1} - \boldsymbol{f}_{s,U}\right) + \boldsymbol{T}_{s,l-1} & \text{on } \Sigma; \end{cases}$$

   (b) The structure subproblem with a Robin condition at the FS interface

$$\begin{cases} \rho_s\dfrac{\xi_{s,0}}{\Delta t^2}\widetilde{\boldsymbol{\eta}}_{s,l} - \nabla\cdot\boldsymbol{T}_{s,l} = \widetilde{\boldsymbol{f}}_s + \rho_s\widetilde{\boldsymbol{f}}_{s,W} & \text{in } \Omega_s^0, \\ \alpha_s\dfrac{\beta_{s,0}}{\Delta t}\widetilde{\gamma}_s\,\widetilde{\boldsymbol{\eta}}_{s,l} - \widetilde{\boldsymbol{T}}_{s,l} \\ \qquad = \alpha_s\widetilde{\gamma}_f\,\widetilde{\boldsymbol{u}}_{f,l} - \widetilde{\boldsymbol{T}}_{f,l}\widetilde{\boldsymbol{n}} + \alpha_s\widetilde{\gamma}_s\widetilde{\boldsymbol{f}}_{s,U} & \text{on } \Sigma^0. \end{cases}$$

The use of two different loops for the geometrical/physical non-linearities and for the imposition of the interface continuity conditions makes this scheme more robust with respect to the use of just a single loop, as shown in [22].

Inexact solutions

In order to improve the performances of Double-loop scheme in terms of CPU time, we report here a family of

algorithms drawn from the *Double-loop* scheme and introduced in [22]. In particular, we consider the *geometrical and convective inexact schemes-m* (GCIS-m), obtained from Double-loop by performing at most m iterations in the external loop, We observe that with GCIS-1 we perform just one external iteration, that is we solve a linearized FSI problem in a known domain (see [4, 7, 10, 23]).

Numerical results

We consider here an application of previous schemes to a real geometry of a patient, namely the human carotid depicted in Figure 2, right. In particular, we want to compare the accuracy of GCIS-1 and GCIS-2 schemes with respect to Double-loop scheme when BDF2 or BDF3 are used for the time discretization of fluid and structure. For GCIS-1 we use a suitable extrapolation of the interface quantities and fluid convective term of order 2 (resp. of order 3) when using BDF2 (resp. BDF3) schemes, in order to recover a global order 2 (resp. 3) as shown in [22]. For GCIS-2 such extrapolation is not necessary to recover order 2 (resp. 3) [22]. The comparison of such schemes when BDF1 discretizations are considered has been already done in [22], highlighting the good accuracy of the inexact schemes.

We use $P1bubble - P1$ finite elements for the fluid subproblem and $P1$ finite elements for the structure subproblem, and the following data: viscosity $\mu = 0.03\,dyne/cm^2$, fluid density $\rho_f = 1\,g/cm^3$, structure density $\rho_s = 1.2\,g/cm^3$, Young modulus $E = 3 \cdot 10^6\,dyne/cm^2$, Poisson ratio $\nu = 0.45$, time discretization parameter $\Delta t = 0.001\,s$, and elastic coefficient of the surrounding tissue $\alpha_e = 3 \cdot 10^6\,dyne/cm^2$. This value has been extracted by the experimental results reported in [19] and allows to recover a pressure in the physiological range.

For the prescription of the interface continuity conditions, in all the simulations we have considered the RR scheme, with the optimal coefficients proposed in [15] and adapted to different temporal schemes in [22].

The results have been obtained with the parallel Finite Element library `LIFEV` developed at MOX - Politecnico di Milano, INRIA - Paris, CMCS - EPF of Lausanne and Emory University - Atlanta.

For the harmonic extension and for the structure, we prescribe at the artificial sections normal homogeneous Dirichlet conditions and tangential homogeneous Neumann conditions, that is we let the domain to move freely in the tangential direction. At the inlet we prescribe the physiological flow-rate depicted in Figure 2, left, through the Lagrange multipliers method [12, 27]. At the outlet, we propose to use the following absorbing boundary condition, obtained by following [22, 23]:

$$\frac{1}{|\Gamma|} \int_\Gamma (\boldsymbol{T}_f\,\boldsymbol{n}) \cdot \boldsymbol{n}\,d\sigma - R_e \int_{\Gamma^n} \boldsymbol{u} \cdot \boldsymbol{n}\,d\sigma = P_{ext} \quad \text{on } \Gamma, \ (9)$$

where $R_e = \sqrt{\frac{\rho_f \tau}{2\sqrt{\pi}}} \frac{1}{A_0^{3/4}}$, $\tau := \frac{EH_s\sqrt{\pi}}{(1-\nu^2)R^2}$, with H_s the structure thickness and R a reference radius. We set $P_{ext} = 0\,mmHg$.
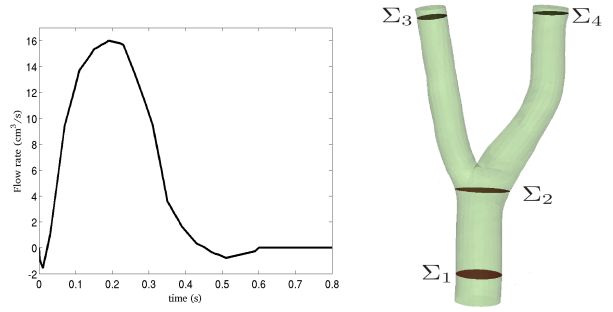
Figure 2 Flow rate waveform prescribed at the inlet of the carotid (left) and fluid domain (right).

We run the simulations on 15 processors for the solution of the fluid problem and on 1 processor for the structure.

We consider four different sections of the domain showed in Figure 2, right. The section Σ_1 is located at $0.05cm$ from the inlet, Σ_2 at $2cm$, Σ_3 at $0.01cm$ from the internal carotid outlet and Σ_4 at $0.2cm$ from the external carotid outlet. For these sections we report, in Figure 3, the flow rate (up) and the mean pressure (bottom) obtained with Double-loop/BDF2. We observe that the flow rate is higher in the internal carotid, as expected since this is the branch which brings the blood to the brain. The pressure varies in the range $70 - 120mmHg$, which corresponds to a typical pressure drop in physiological conditions.
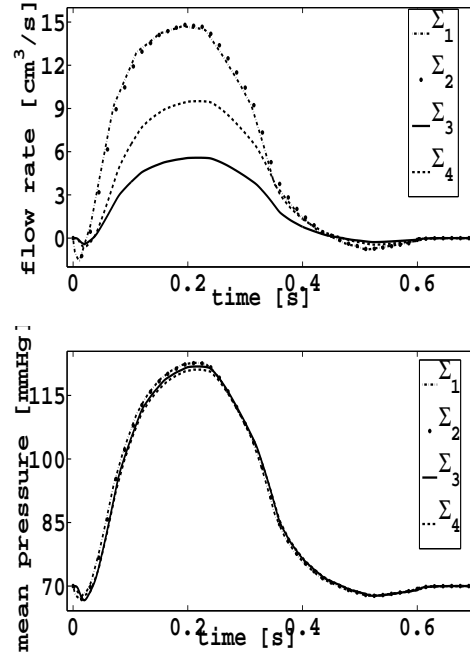
Figure 3 Flow rate (in cm^3/s, up) and mean pressure (in $mmHg$, bottom) at different sections.

In Figure 4 we report the wall shear stress (WSS) and the fluid velocity at the peak instant, obtained with Double loop/BDF2. The results obtained with GCIS-1 and GCIS-2
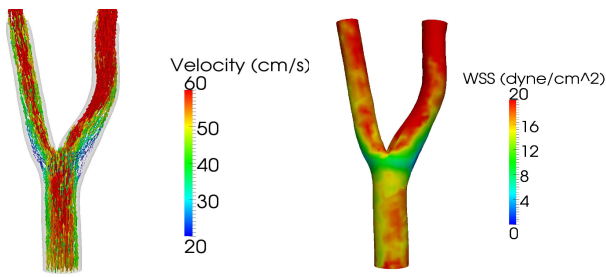
Figure 4 Fluid velocity field (left) and wall shear stress (right) at the peak instant.

and with BDF3 are very similar to those reported in Figure 4, so that we do not report them here. In order to quantify the differences, we define the following percentage error with respect to Double-loop solution

$$E_x = \frac{\|x_{DL} - x_*\|_{L^\infty(\Omega^t)}}{\|x_{DL}\|_{L^\infty(\Omega^t)}} \times 100, \qquad (10)$$

where x represents one of the quantities WSS, fluid velocity, fluid pressure and solid displacement, DL stands for Double-loop and $*$ for one of the other scheme. Of course, the errors of GCIS-1 and GCIS-2 obtained by using BDFq schemes, $q = 2, 3$, are computed with respect to the Double Loop solution obtained with BDFq schemes. In Table 1 we report these errors at the peak instant. We observe

	E_{WSS}	E_{η_s}	E_{u_f}	E_{p_f}
GCIS-1/BDF2	0.37	0.29	0.14	0.15
GCIS-2/BDF2	0.047	0.004	0.005	0.002
GCIS-1/BDF3	5.42	5.22	5.24	5.83
GCIS-2/BDF3	0.29	0.03	0.07	0.08

Table 1 Percentage error of GCIS-1 and GCIS-2 with respect to the Double-loop solution for BDF2 and BDF3. Computation done with (10) **at the peak instant.**

a quite good accuracy when using BDF2 schemes, expecially for GCIS-2. Viceversa, relative errors obtained with BDF3 are more than one order of magnitude greater than those obtained with BDF2. In this case, the accuracy of GCIS-1 seems to be not good.

In Table 2 we report the CPU time normalized with respect to that of Double-loop scheme for BDF2 and BDF3. We observe that Double-loop is about 3 times more expen-

	BDF2	BDF3
GCIS-1	0.31	0.32
GCIS-2	0.46	0.47

Table 2 CPU time normalized with respect to that of Double-loop scheme for BDF2 and BDF3

sive than GCIS-1 and more than 2 times more expensive than GCIS-2, and that the normalized CPU time seems to be independent of the temporal scheme.

In conclusion, we can state that GCIS-2 scheme is an effective algorithm for the solution of real haemodynamic problems for second and third order accurate temporal schemes. Indeed, it features a good accuracy with respect to the solution obtained with Double-loop, used here as gold-standard, and a satisfactory improvement in the CPU time (halving the time with respect to Double-loop). These results confirms the nice features of GCIS-2 scheme for real applications highlighted in [22] for a first order temporal scheme.

Acknowledgments

References

[1] M. Astorino, F. Chouly, and M. Fernández. Robin based semi-implicit coupling in fluid-structure interaction: stability analysis and numerics. *SIAM J Sc Comp*, (31(6)):4041–4065, 2009.

[2] S. Badia, F. Nobile, and C. Vergara. Fluid-structure partitioned procedures based on Robin transmission conditions. *Journal of Computational Physics*, 227:7027–7051, 2008.

[3] S. Badia, F. Nobile, and C. Vergara. Robin-Robin preconditioned Krylov methods for fluid-structure interaction problems. *Computer Methods in Applied Mechanics and Engineering*, 198(33-36):2768–2784, 2009.

[4] S. Badia, A. Quaini, and A. Quarteroni. Splitting methods based on algebraic factorization for fluid-structure interaction. *SIAM J Sc Comp*, 30(4):1778–1805, 2008.

[5] Y. Bazilevs, V. Calo, Y. Zhang, and T. Hughes. Isogeometric fluid-structure interaction analysis with applications to arterial blood flow. *Computational Mechanics*, 38:310–322, 2006.

[6] P. Causin, J. Gerbeau, and F. Nobile. Added-mass effect in the design of partitioned algorithms for fluid-structure problems. *Computer Methods in Applied Mechanics and Engineering*, 194(42-44):4506–4527, 2005.

[7] P. Crosetto, S. Deparis, G. Fourestey, and A. Quarteroni. Parallel algorithms for fluid-structure interaction problems in haemodynamics. *EPFL-REPORT-148536*, 2009.

[8] S. Deparis, M. Discacciati, G. Fourestey, and A. Quarteroni. Fluid-structure algorithms based on Steklov-Poincaré operators. *Computer Methods in Applied Mechanics and Engineering*, 195(41-43):5797–5812, 2006.

[9] J. Donea. An arbitrary Lagrangian-Eulerian finite element method for transient dynamic fluid-structure interaction. *Computer Methods in Applied Mechanics and Engineering*, 33:689–723, 1982.

[10] M. Fernández, J. Gerbeau, and C. Grandmont. A projection semi-implicit scheme for the coupling of an elastic structure with an incompressible fluid. *Inter-*

national Journal for Numerical Methods in Engineering, 69(4):794–821, 2007.

[11] C. Figueroa, I. Vignon-Clementel, K. Jansen, T. Hughes, and C. Taylor. A coupled momentum method for modeling blood flow in three-dimensional deformable arteries. *Computer Methods in Applied Mechanics and Engineering*, 195:5685–5706, 2006.

[12] L. Formaggia, J.-F. Gerbeau, F. Nobile, and A. Quarteroni. Numerical treatment of defective boundary conditions for the Navier-Stokes equation. *SIAM Journal on Numerical Analysis*, 40(1):376–401, 2002.

[13] L. Formaggia, A. Quarteroni, and A. V. (Eds.). *Cardiovascular Mathematics - Modeling and simulation of the circulatory system*. Springer, 2009.

[14] C. Forster, W. Wall, and E. Ramm. Artificial added mass instabilities in sequential staggered coupling of nonlinear structures and incompressible viscous flow. *Computer Methods in Applied Mechanics and Engineering*, 196(7):1278–1293, 2007.

[15] L. G. Giorda, F. Nobile, and C. Vergara. Analysis and optimization of robin-robin partitioned procedures in fluid-structure interaction problems. *SIAM Journal on Numerical Analysis*, 48(6):2091–2116, 2010.

[16] E. Hairer, S. Nørsett, and G. Wanner. *Solving ordinary differential equations: Nonstiff problems*. Springer series in computational mathematics. Springer, 1993.

[17] E. Hairer and G. Wanner. *Solving Ordinary Differential Equations II: Stiff and Differential-Algebraic Problems*. Springer Series in Computational Mathematics. Springer, 2010.

[18] T. J. R. Hughes, W. K. Liu, and T. K. Zimmermann. Lagrangian-Eulerian finite element formulation for incompressible viscous flows. *Computer Methods in Applied Mechanics and Engineering*, 29(3):329–349, 1981.

[19] Y. Liu, C. Charles, M. Gracia, H. Gregersen, and G. S. Kassab. Surrounding tissues affect the passive mechanics of the vessel wall: theory and experiment. *Am J Physiol Heart Circ Physiol*, 293:H3290–H3300, 2007.

[20] P. Moireau, N. Xiao, M. Astorino, C. A. Figueroa, D. Chapelle, C. A. Taylor, and J.-F. Gerbeau. External tissue support and fluid-structure simulation in blood flows. *Biomechanics and Modeling in Mechanobiology*, 2011.

[21] F. Nobile. *Numerical approximation of fluid-structure interaction problems with application to haemodynamics*. PhD thesis, École Polytechnique Fédérale de Lausanne, 2001. Thesis n° 2458.

[22] F. Nobile, M. Pozzoli, and C. Vergara. Time accurate partitioned algorithms for the solution of fluid-structure interaction problems in haemodynamics. Submitted.

[23] F. Nobile and C. Vergara. An effective fluid-structure interaction formulation for vascular dynamics by generalized Robin conditions. *SIAM J Sc Comp*, 30(2):731–763, 2008.

[24] K. Perktold, E. Thurner, and T. Kenner. Flow and stress characteristics in rigid walled and compliant carotid artery bifurcation models. *Medical and Biological Engineering and Computing*, 32(1):19–26, 1994.

[25] S. Piperno and C. Farhat. Design of efficient partitioned procedures for transient solution of aerolastic problems. *Rev. Eur. Elements Finis*, 9(6-7):655–680, 2000.

[26] T. Tezduyar, S. Sathe, T. Cragin, B. Nanna, B. Conklin, J. Pausewang, and M. Schwaab. Modelling of fluid-structure interactions with the space-time finite elements: arterial fluid mechanics. *International Journal for Numerical Methods in Fluids*, 54:901–922, 2007.

[27] A. Veneziani and C. Vergara. Flow rate defective boundary conditions in haemodinamics simulations. *International Journal for Numerical Methods in Fluids*, 47:803–816, 2005.